International Journal of Engineering Research & Technology (IJERT)
ISSN: 2278-0181
Vol. 8 Issue 11, November-2019

Interconnection of Weak Power System by VSC-HVDC using Fuzzy based Compensation Control

G. Saraswathi
Professor, EEE, JNTUK-UCEV
Vizianagaram, Andhra Pradesh,
India.

Srilekha. V
P. G. Student, EEE, JNTUK-UCEV
Visakhapatnam, Andhra Pradesh,
India.

Abstract **: To enhance the power transmission capability and stability using VSCs became an attractive alternative technology. This paper proposes and addresses a Fuzzy based power compensation control to interconnection of weak power systems by VSC-HVDC. This proposed new control methodology improves the damping control performance of the active power and the AC voltage by adjusting the compensated values based on analysis and characteristics of PV curves. Small signal model of the integrated system is established to study the performance of the proposed control method. The impact of the compensation coefficients and steady state operating points on the system stability is studied. Electromagnetic transient simulation models are considered and verified in MATLAB / Simulink environment for the effectiveness of the method on the performance of operating limits, damping performance, disturbance withstanding capability, and fault ride-through capability.**

***Index Terms—Voltage source converter (VSC), HVDC, weak power system, power compensation control, stability analysis, small signal modeling, virtual impedance*.**

NOMENCLATURE

C_f Reactive power compensation capacitor
P,Q Active- and reactive power at PCC
δ Angle difference between U_{gabc} and U_{sabc}
Ug Phase voltage amplitude of grid source
Us Phase voltage amplitude at PCC
Z_t Transformer impedance
Q_s Reactive power output of VSC
Q_c Reactive power generated by C_f
P_{ref} References of active power for inner Current reference calculation
Q_{ref} References of reactive power for inner current reference calculation
Q_0 Steady state reactive power
P_0 Steady state active power, P_0=P*
I_{sd0} , I_{sq0} Steady state *d*-and *q*-axis current of VSC
I_{gd0} , I_{gq0} Steady state *d*-and *q*-axis grid current
Z_{gvir} Grid current virtual impedance
Z_{svir} VSC current virtual impedance
$F_{PLL(s)}$ Closed-loop transfer function of PLL
θ Angle outputted from PLL
$G_{auc(s)}$ Transfer function of PI regulator
Z_g, R_g, X_g Grid equivalent Impedance, Resistance, Reactance

I. INTRODUCTION

For reduction of cost and improved reliability, most of the world's electric power systems continue to be interconnected. Interconnections take advantage of diversity of loads, availability of sources and fuel price for supplying power to loads at minimum cost and pollution with a required reliability. In a deregulated electric service environment, an effective electric grid is essential to the competitive environment of reliable electrical service[1]. Increased demands on transmission, absence of long-term planning, and the need to provide open access to generating companies and customers have resulted in less security and reduced quality of supply[2]. Compensation in power systems is, therefore, essential to alleviate some of these problems. Series/shunt compensation has been in use for past many years to achieve this objective. Load compensation is the management of reactive power to improve the quality of supply especially the voltage and p.f levels. Here the reactive power is adjusted with respect to an individual load and the compensating device is connected to the load itself.

Interconnection between AC and DC networks has become the attractive solution by using Voltage-source converters (VSCs) . It has been widely used in many applications, such as integration of renewable energy generation [4], high-voltage direct current (HVDC) transmission [5] and back-to-back systems, integration of energy storage systems [6], and railway traction systems [7]. The VSC-HVDC technology has been proposed as a promising solution for a back-to-back project in China to interconnect a weak AC power system to a strong AC system [8]-[11].

LC or *LCL* output filters are usually adopted to mitigate the converter switching ripples. However, if the converters are not properly controlled, inherent resonances of the filters can introduce serious power quality and stability problems [7]. Power-angle control has been studied for HVDC, static-synchronous- compensator (STATCOM), and wind-turbine applications. But the disadvantage of power-angle control is that the control bandwidth is limited by a resonant peak at the grid frequency and the control system does not have the capability to limit the current flowing into the converter.[8] The pulse-width modulation (PWM) based voltage-source converter (VSC) is an emerging technology for HVDC transmission [16], [17]. In contrast to the conventional thyristor-based HVDC system, a VSC-HVDC system has the potential to be connected to very weak ac systems, as well as the capability to generate or consume reactive power depending on the operating conditions. Synchronous condensers have to be installed to increase the short-circuit capacity of the ac system. However, synchronous condensers can substantially increase the investment and maintenance costs of an HVDC project [11].

To enhance the power transmission capability of a VSC-HVDC connected to a very weak power system. Some control strategies were introduced such as power synchronization control (PSC) [8]-[11], [16], virtual synchro-converter control [6], [15], [17]-[19], and advanced vector control [11]. The operating performance of the VSC-HVDC that is interconnected with a weak power system was investigated in [11], which indicates that the stability of the VSC was mainly affected by the phase angle difference of the AC voltage when AC voltage control mode was adopted. Hence, to improve the power transmission capability PSC method was adopted. A backup PLL was needed for synchronous loop under AC system faults. Since the power controller has the capability of regulating the AC voltage and frequency, the proposed control method provided an effective solution for large-scale renewable integration. However, the control method did not provide a solution for the interconnection of a weak power system. A series of control strategies such as nonlinear power damping controller [15], comprehensive control framework [18], and multi-variable droop control [19] were proposed to imitate VSCs as synchronous machines for integrating renewable power generation into weak power systems.

The virtual synchro-converter control and PSC can provide great control performance for a VSC-HVDC system. In order to enhance the transmission capability, dominant control strategy has been used for the practical applications is the vector control comprising an outer loop and an inner loop [11]. Conclusions drawn in [11] indicates that it was the outer loop limits the power transmission capability when compare with the inner current loop. An advanced current vector control method was presented using a novel outer loop. During the dynamic state the parameters of the outer loop controllers designed using the H-infinity method needs to be updated.

A ± 420kV/1250MW back-to-back VSC-HVDC project is planned to interconnect the AC systems between Chongqing City and Hubei Province in China. The project is proposed to employ symmetrical monopole configuration based on modular multilevel converter (MMC) topology. The main purpose of this paper is to improve the stability of the project. To restrain the AC system resonance, active damping impedance has been combined in the inner loop, such that this control strategy which automatically adjusts the compensated values. Corresponding small signal modeling is established and the performance of the proposed method is studied.

II. SYSTEM MODEL

A VSC-HVDC system is presented in Fig. 1, where the basic controller for the rectifier and inverter stations are also presented. Normally, power is sent from the rectifier station to the inverter station. Power control is implemented at the rectifier station, while the inverter station controls dc-link voltage to ensure power balance. An advantage of VSC-HVDC over line commutated Converters HVDC (LCC-HVDC) is its reactive power compensation capability, which is provided by the reactive power controller or ac voltage controller [21].

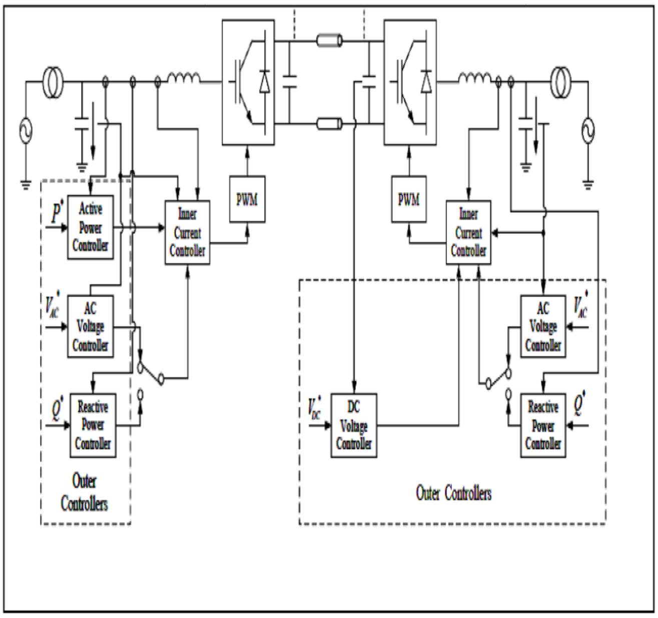

Fig.1: Two terminal VSC-HVDC system

For a balanced three-phase system, Fig. 2 shows the equivalent circuit of a VSC connecting with an ac grid via a coupling inductor, where the resistor is neglected. The ac grid is modeled as an ac voltage source with an impedance.

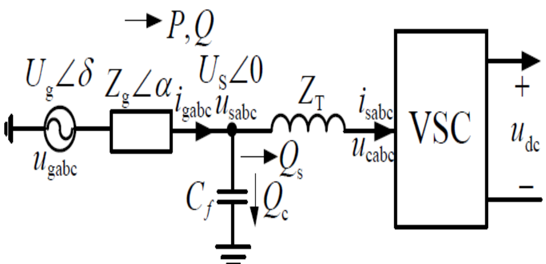

Fig.2: Equivalent circuit representation of a VSC

$$P = \frac{U_s U_g}{Z_g} \sin\delta \qquad (1)$$

$$Q = \frac{U_g^2 - U_s U_g \cos\delta}{Z_g} \qquad (2)$$

Where, P and Q are the active and reactive powers between two electrical nodes in ac systems with voltage magnitudes

International Journal of Engineering Research & Technology (IJERT)
ISSN: 2278-0181
Vol. 8 Issue 11, November-2019

U_s and U_g. The quantities δ and Z_g are the phase-angle difference and line impedance between the two nodes. From (1 &2) it follows that the active power is mainly related to the phase angle δ, while the reactive power is more related to the voltage-magnitude difference. i.e., the active power is controlled by the phase angle of the VSC voltage, while the reactive power is controlled by the magnitude of the VSC voltage

A. Characteristics of Weak AC Systems

A weak ac system characterized typically by its high impedance [8]. As the ac-system impedance increases, the voltage magnitude of the ac system will become more sensitive to power variations of the HVDC system. The difficulty is measured by the short-circuit ratio (SCR), which is defined as a ratio of the ac-system short-circuit capacity to the rated power of the HVDC system

$$\text{SCR}=\frac{S_{ac}}{P_{dn}} \tag{3}$$

where, S_{ac} is the short-circuit capacity of the ac system at the filter bus, P_{dn} is the rated dc power of the HVDC link.

B. Operating limits

When operating a VSC-HVDC link, it is essential to take into account the limitations of the converter in terms of active and reactive power transfer capability. One of the limit is the converter-current limitation, which is imposed by the current rating of the converter valve. Since both the active power and reactive power contribute to the current flowing through the valve, this limitation is manifested as a circle.

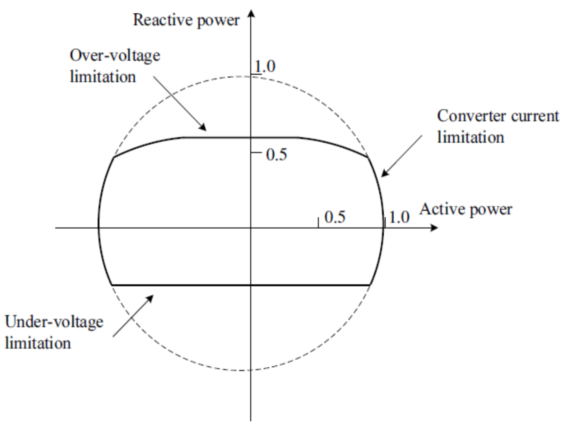

Fig.3: Operation limitation of a typical VSC- HVDC converter

Accordingly, if the converter is intended to support the ac system with reactive power supply/consumption, the maximum active power has to be limited to make sure that the converter current is within the limit. Another limitation which determines the reactive-power capability of the VSC is the over or under-voltage magnitude of the VSC. The over-voltage limitation is imposed by the direct voltage level of the VSC. The under-voltage limit, however, is limited by the active-power transfer capability, which requires a minimum voltage magnitude to transmit the active power. Fig. 3 represents the PQ diagram for a typical VSC-HVDC converter [9].

This phenomenon indicates that the PCC needs to absorb reactive power to keep the AC voltage under steady states. Another important phenomenon is that the reactive power is not significantly required when $|P| < 0.5$ (i.e. $|\delta| < 30°$) [9].However, its demand increases dramatically when $|P|>0.5$ (i.e.$|\delta|>30°$) especially in the high power level range (|i.e. $P|> 0.7$, $|\delta|>45°$) due to the strong nonlinearity of weak power system (SCR=1). Therefore, the reactive power providing capability of VSCs which interconnect with a very weak power system determine the dynamic performance of the weak power system. With dramatically increased demand for reactive power, a capacitor Cf is connected to the PCC to prevent the VSC from over current under steady states in practical applications.

III. PV curve analysis

The impact of active power on the PCC voltage can be unambiguously demonstrated by the natural PV analysis. To clarify the dynamic process, we suppose that only one regulator in the two channels is enabled during the dynamic states. The first progress enables the power control loop with reactive power unchanged. The second progress enables the AC voltage control loop with active power unchanged.

In the first progress, that the value of the phase angle difference δ increases due to

$$\delta = \sin^{-1}\frac{P}{U_s} \tag{4}$$

In the second state, the active power holds unchanged and the AC voltage controller regulates the q-axis current to produce more reactive power to the PCC.

The response speed of the reactive power injected into the PCC determines the fluctuation of the PCC voltage in the analyzed dynamic process. However, the response speed of the reactive power is directly related to the AC voltage loop. Hence, whether the response speed of the AC voltage loop can match that of the active power loop will determine the system performance when the active power changes from a low level to a higher level. Consequently, reducing the response speed of the active power and improving the response speed of the AC voltage loop are a reliable way to restrain the fluctuation of the PCC voltage and enhance the system stability when the VSC is interconnected with a very weak power system.

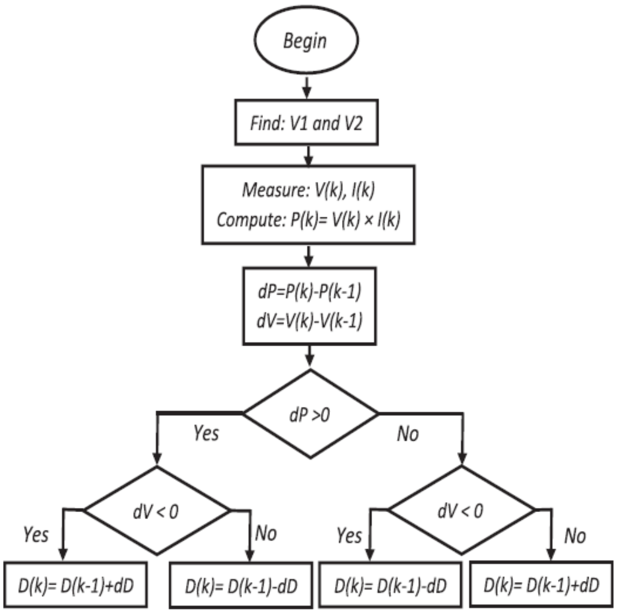

Fig.4: Flowchart for perturbation and observation technique.

IV. COMPENSATION STRATEGY

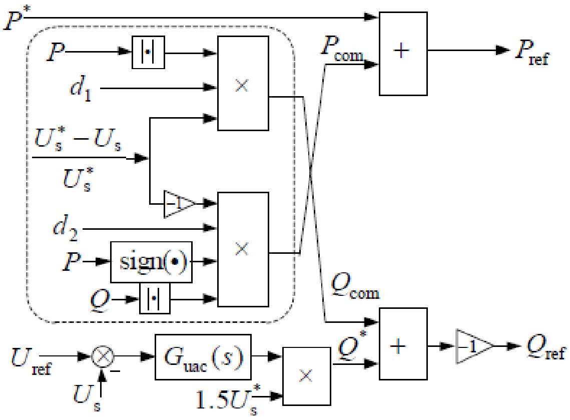

Fig.5: outer loop of compensation strategy

A new control strategy which can achieve two objectives. One is that it would be better for the new control strategy to have the ability to restrain the rate of response of the active power. By doing so, more time is left to the AC voltage controller to generate corresponding reactive power. The other one is that control method should have the ability to enhance the response of the AC voltage loop to suppress the PCC voltage fluctuation[3].

In Fig.5, *P** is the commanded active power ordered from the dispatching center, *P*ref is the active power from outer loop (*P*ref =*P** in steady state). |·| is the operation for absolute value, sign(·) is sign function, *P*com and *Q*com are the compensated values of the active and reactive power, respectively. From the structure of the proposed method, it uses the product of the PCC voltage fluctuations and instantaneous power to generate the compensated power automatically. Hence, it does not need to dynamically adjust the compensation coefficients based on the transmitted active power level when compared to [9].

The expression for compensated power can be written as,

$$P_{com} = \frac{U_s^* - U_s}{U_s^*} |Q|.\,sign(p).\,d_2 \qquad (5)$$

$$Q_{com} = \frac{U_s^* - U_s}{U_s^*} |P|.\,d_1 \qquad (6)$$

The reference values of active and reactive power generated from outer loop can be expressed as

$$P_{ref} = P^* + P_{com} \qquad (7)$$

$$Q_{ref} = -Q^* - Q_{com} \qquad (8)$$

$$Q^* = 1.5U_s^* G_{uac}(s)(U_{ref} - U_s) \qquad (9)$$

$$U_{ref} = U_s^* + (U_s^* - U_s)d_3 \qquad (10)$$

Where, $G_{uac}(s)$ is the transfer function of PI regulator. d_1 and d_2 are the damping compensation coefficients. d_3 is the tuning coefficient for the AC voltage loop

a) Current control: The VSC-HVDC system consists of two terminal stations: one is the rectifier station and the other is the inverter station. Fig. 6 presents the controller of the rectifier station, in which active power P_{ref} and reactive power Q_{ref} are to be regulated. Depending on the requirements of the application, the reactive power control could be substituted with ac grid voltage control. U_{sd} and U_{sq} are the converter output voltages and could be derived as (11) &(12), which is essentially the inner current control loop.[24]

$$u_{cd}^* = u_{sd} - G_{isd}(i_{sd}^* - i_{sd}) + wL_1 i_{sq} + Z_{gvir} i_{gd} + Z_{svir} i_{sd} \quad (11)$$

$$u_{cq}^* = u_{sq} - G_{isq}(i_{sq}^* - i_{sq}) + wL_1 i_{sq} + Z_{gvir} i_{gq} + Z_{svir} i_{sq} \quad (12)$$

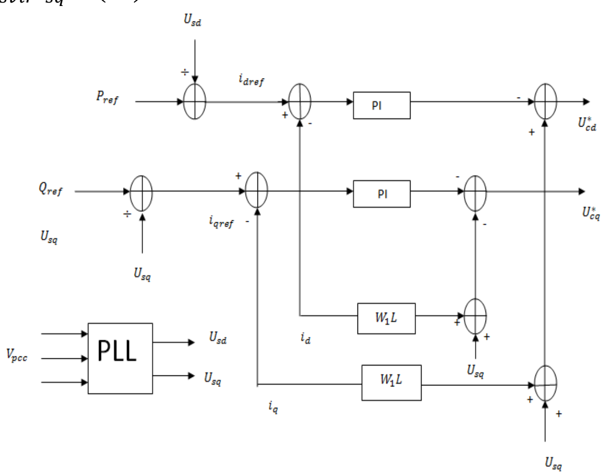

Fig.6: Controller of the rectifier station

The currents in the inner loop can be written as

$$i_{sd}^* = 2P_{ref}/3(u_{sd}^{cs}) \qquad (13)$$

$$i_{sq}^* = 2Q_{ref}/3(u_{sd}^{cs}) \qquad (14)$$

The active damping impedances are described as follows

$$Z_{gvir} = R_{gvir} + \frac{k_g.s}{s+w_{gc}} \qquad (15)$$

$$Z_{svir} = R_{svir} + \frac{k_s.s}{s+w_{sc}} \qquad (16)$$

Where, R_{gvir} and R_{svir} are the active damping resistors

k_g and k_s are the gain coefficients of the HPFs

w_{gc} and w_{sc} are the bandwidths

$$G_{isd} = G_{isq} = K_p + \frac{K_i}{s}$$

International Journal of Engineering Research & Technology (IJERT)
ISSN: 2278-0181
Vol. 8 Issue 11, November-2019

G_{isd} and G_{isq} are the PI regulators of current loop in d and q axis.

b) ***Power control***: The rectifier station controls the active power transferred from the left-hand side grid to the converter, which is the outer control loop in dual *dq* control loops. Equation (17) computes the *d* -axis current reference that controls the active power flow

$$i_{dref} = \frac{2}{3}\frac{P_{ref}}{U_{sdo}} \quad (17)$$

The small-signal representation of the -axis current reference is then expressed as follows:

$$\Delta i_{dref} = -\frac{2}{3}\frac{P_{ref}}{U_{sdo}^2}[\,\Delta U_s - \Delta U_s^*] \quad (18)$$

Where, U_{sdo} is the rectifier PCC steady-state voltage. Since the direct reactive power compensation control is used throughout this paper, the q-axis current reference can be derived similarly as above

$$i_{qref} = -\frac{2}{3}\frac{Q_{ref}}{U_{sqo}} \quad (19)$$

$$\Delta i_{qref} = \frac{2}{3}\frac{Q_{ref}}{U_{sdo}^2}[\,\Delta U_s - \Delta U_s^*] \quad (20)$$

c) DC voltage control: The inverter station regulates the dc-link voltage and maintains the active power balance. The inner current control loop is identical to the rectifier station shown in Fig. 3, whereas the outer loop is replaced by a dc voltage controller. The dc voltage controller is a typical PI controller.

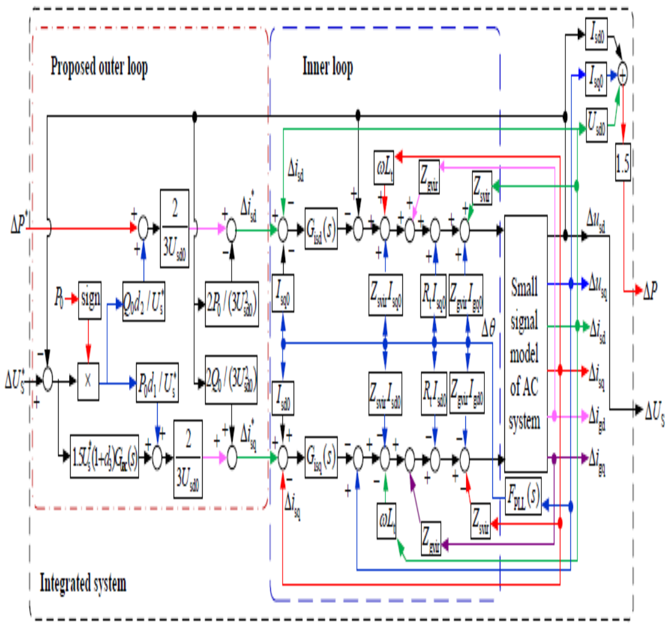

Fig.7 Small signal model of the integrated system with the proposed method

Considering the dynamics on dc capacitor c_{dc}, the energy stored in the capacitor is

$$W = \frac{1}{2}C_{dc}v_{dc}^2 \quad (21)$$

$$\frac{1}{2}\,C_{dc}\frac{dv_{dc}^2}{dt} = P - P_L = P_{dc} \quad (22)$$

$$v_{dc}\frac{dv_{dc}}{dt} = P - P_L \quad (23)$$

V. PROPOSED METHOD

Fuzzy Logic Control: L. A. Zadeh presented the first paper on fuzzy set theory in 1965. Since then, a new language was developed to describe the fuzzy properties of reality, which are very difficult and sometime even impossible to be described using conventional methods. Fuzzy set theory has been widely used in the control area with some application to power system [29]. A simple fuzzy logic control is built up by a group of rules based on the human knowledge of system behavior. Matlab/Simulink simulation model is built to study the dynamic behavior of converter. Furthermore, design of fuzzy logic controller can provide desirable both small signal and large signal dynamic performance at same time, which is not possible with linear control technique. Thus, fuzzy logic controller has been potential ability to improve the robustness of compensator.

The basic scheme of a fuzzy logic controller is shown in Fig 8 and consists of four principal components such as: a fuzzification interface, which converts input data into suitable linguistic values; a knowledge base, which consists of a data base with the necessary linguistic definitions and the control rule set; a decision-making logic which simulating a human decision process, infer the fuzzy control action from the knowledge of the control rules and linguistic definitions; a de-fuzzification interface which yields non fuzzy control action from an inferred fuzzy control action [29].

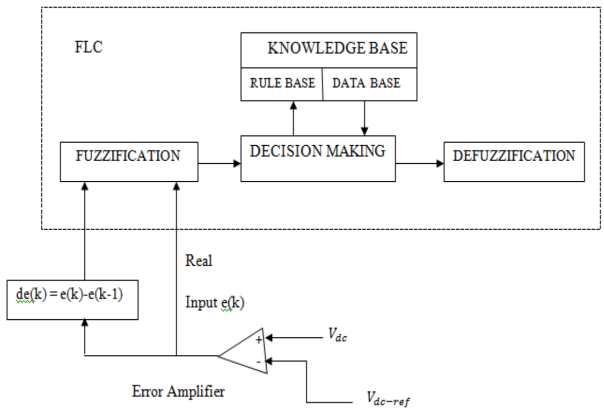

Fig.8. Block diagram of the Fuzzy Logic Controller (FLC) for Proposed method

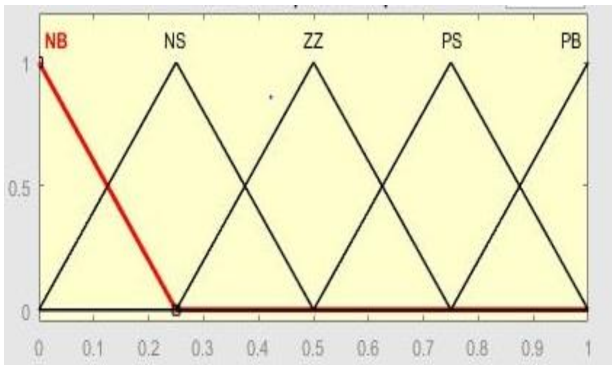

Fig.9. Membership function of input, change in input

International Journal of Engineering Research & Technology (IJERT)
ISSN: 2278-0181
Vol. 8 Issue 11, November-2019

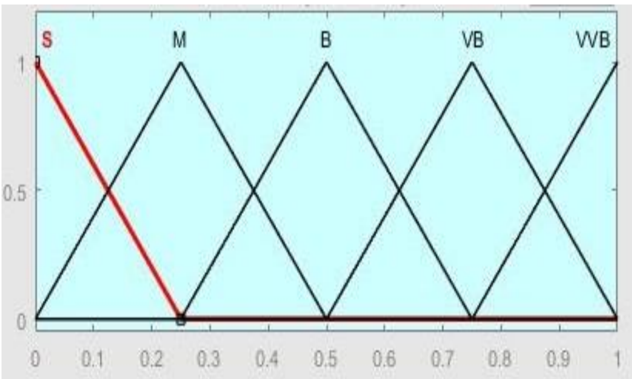

Fig.10. Membership function of output

Rule Base: The elements of this rule base table are determined based on the theory that in the transient state, large errors need coarse control, which requires coarse input/output variables; in the steady state, small errors need fine control, which requires fine input/output variables. Based on this the elements of the rule table are obtained as shown in Table, with "*Vdc*" and "*Vdc-ref*" as inputs

Table1.1 Rule Base Table of 5*5 Matrix

de \ e	NB	NS	ZZ	PS	PB
NB	S	S	M	M	B
NS	S	M	M	B	VB
ZZ	M	M	B	VB	VB
PS	M	B	VB	VB	VVB
PB	B	VB	VB	VVB	VVB

VI. SIMULATION RESULTS:

1.Dynamic Performance Analysis:

The system with compensation method of AC voltage loop has a faster response than of without compensation method. It should be noted that enlarging the parameters of AC voltage PI regulator is able to accelerate the response speed of the without compensation. However, this is limited to a narrow range since it is easy to bring oscillatory instability if the system is underdamped

Table 1.2 Dynamic Response comparison

	Active Power Step		PCC Voltage Step	
Time(ms)	Without Compensation	With Compensation	Without Compensation	With Compensation
Rising Time(t_r)	27	63	57	18
Settling time(t_s)	109	116	193	132

2 Stability Performance Analysis: The stability performance is analyzed by taking the configurations for the electromagnetic simulation model. The active power reference *P** ordered from the dispatching center steps -0.1 p.u. per 0.5s for both methods. The parameters of PI regulator are taken as K_{pac} = 0.005 , K_{iac} = 0.05 and the parameters of AC voltage regulator are taken as K_{pac} = 0.035 , K_{iac} = 0.35 and the corresponding waveforms are plotted as shown in fig . However with this method of compensation strategy it presents satisfactory performance with PCC voltage almost unchanged during dynamic process.

3 Stability limit simulation: The operating limits of electromangentic transient model are tested in both rectifier and inverter mode. The first graph plots the active power generated from the VSC. The PCC voltage in the middle graph. In the first dynamic process, voltage continuously sags before t=2.15s because $|Q_c + Q_s| < |Q|$and it gradually restores to steady point around *t*=2.54s.. (rectifier mode) In second dynamic process, voltage increased to maximum value 1.21p.u at t=4.06s due to $|Q_c + Q_s| > |Q|$.(inverter mode).

4 Damping Performance Analysis: The damping performance of the method is simulated in order to validate the system as it cannot operate in steady state if a single virtual impedance is adopted. Two cases are studied i.e accelerating stability(P= -1.04p.u) and oscillatory stability. (P= 0.94p.u) . The system does not become unstable as long as δ does not exceed its limited values. The practical situations of the weak power system are simulated i.e. NPS and PPS are superimposed to fundamental voltage. Based on such operating conditions, four desired active power, *P**=0.67p.u. and *P**=0.4p.u. in rectifier mode, *P**=-0.74p.u. and *P**=-0.4p.u. in inverter mode are simulated.

5 Disturbance Rejection Capability Analysis: The practical situations of the weak power system are simulated i.e. NPS and PPS are superimposed to fundamental voltage. Based on such operating conditions, the rectifier and inverter mode waveforms are plotted as follows

6 Fault Ride through Capability: When two percent 5^{th} Negative Phase Sequence(NPS) and one percent 7^{th} Positive Phase Sequence(PPS) harmonics are superimposed to the fundamental voltage to simulate the practical power grid.

MAIN PARAMETERS OF CIRCUIT AND CONTROL SYSTEM:

Parameters	*Values*
DC voltage	$\pm 420KV$
Rated AC voltage (RMS)	525KV
Rated active power	1250MW
Grid impedance(SCR=1)	220.5Ω
Compensation capacitor	$4.1\mu F$
Transformer leakage	0.098H
Inductance per arm	140mH
d_1 , d_2 , d_3	2.5 ,1.5,6
K_{pac}	0.005
K_{iac}	0.05
R_{svir}	0.45
R_{gvir}	2.95
K_s , W_{sc}	0,0.6
K_g , W_{gc}	0.45,0.6

International Journal of Engineering Research & Technology (IJERT)
ISSN: 2278-0181
Vol. 8 Issue 11, November-2019

Case1: PI Controller

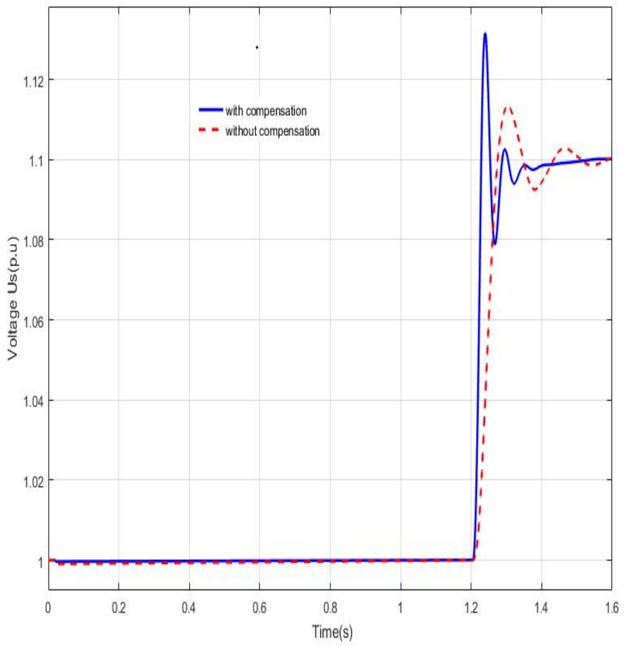

Fig 11 PCC Voltage Steps to 0.1p.u with and without compensation

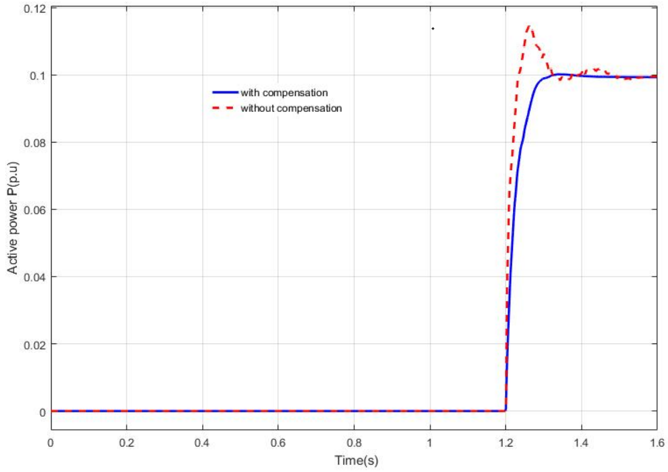

Fig 12 Active Power Steps to 0.1p.u with and without compensation

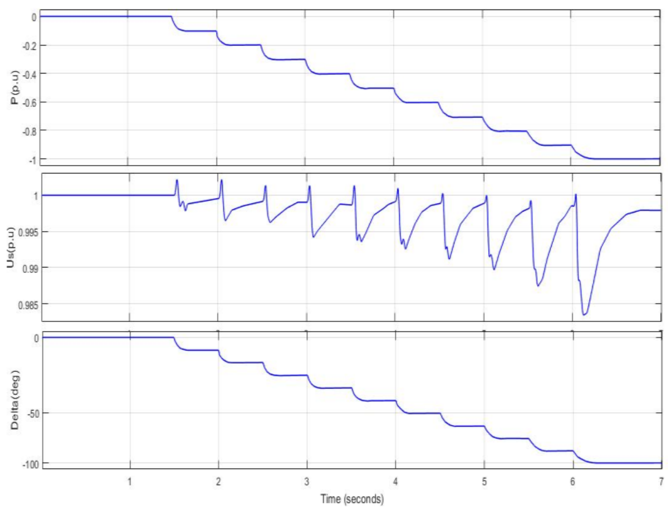

Fig.13 Stability Performance of system upper: active power at PCC; middle: PCC voltage; lower: phase angle δ.when K_{pac} = 0.005 , K_{iac} = 0.05

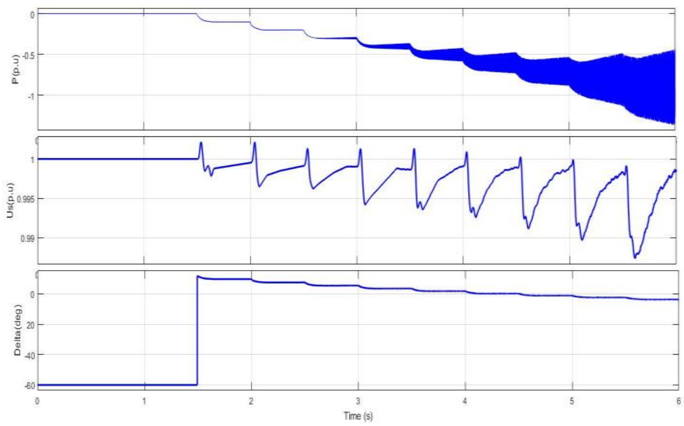

Fig.14 Stability Performance of system upper: active power at PCC; middle: PCC voltage; lower: phase angle δ. when K_{pac} = 0.035 , K_{iac} = 0.35

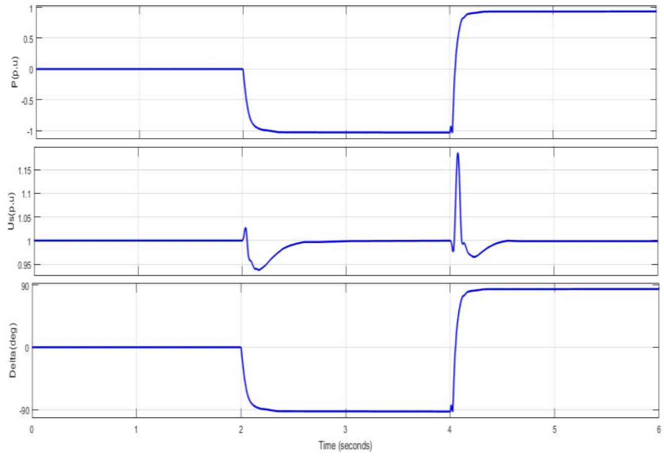

Fig.15 Limits testing of the method. Upper: active and reactive power injected by VSC; middle: PCC voltage; lower: phase angle δ.

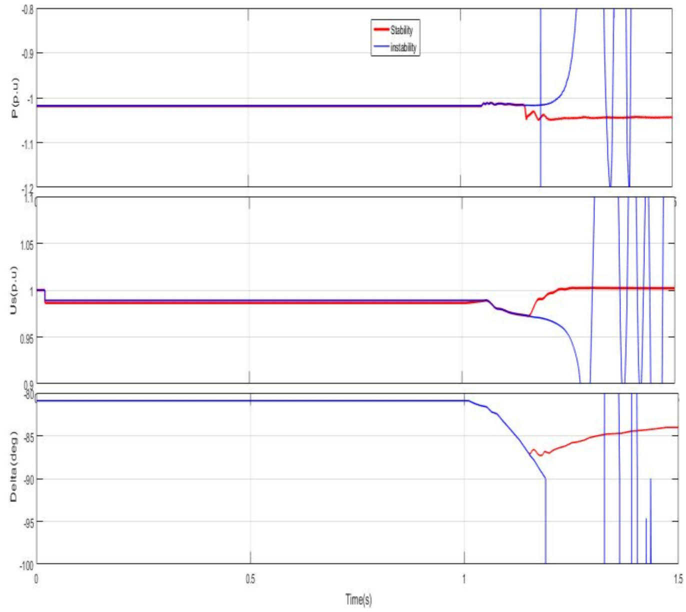

Fig.16 Damping performance of the system for the step value of P= 1.04p.u upper: active power at PCC; middle: PCC voltage; lower: phase angle δ

International Journal of Engineering Research & Technology (IJERT)
ISSN: 2278-0181
Vol. 8 Issue 11, November-2019

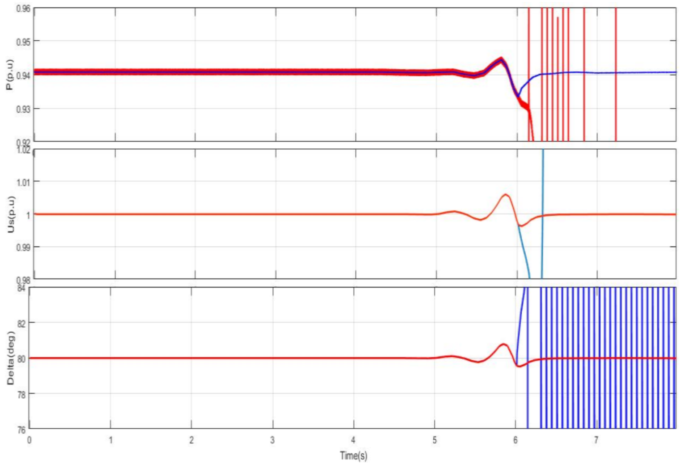

Fig.17 Damping performance of the system for the step value of P = 0.94p.u upper: active power at PCC; middle: PCC voltage; lower: phase angle δ.

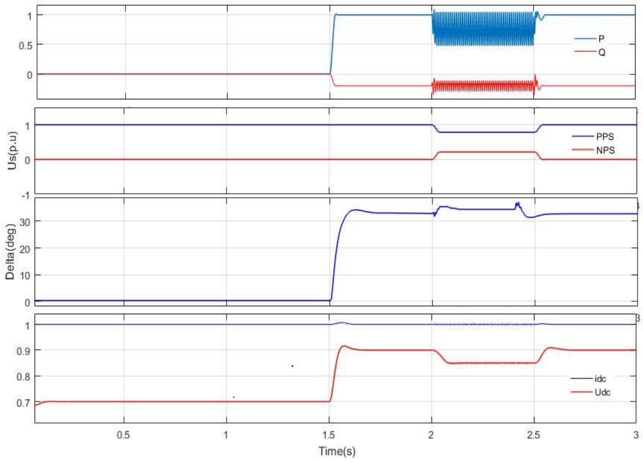

Fig.20 Fault ride-through performance of the proposed method. First: active and reactive power, second: voltages of PPS and NPS; third: phase angle δ; fourth: DC voltage and current.

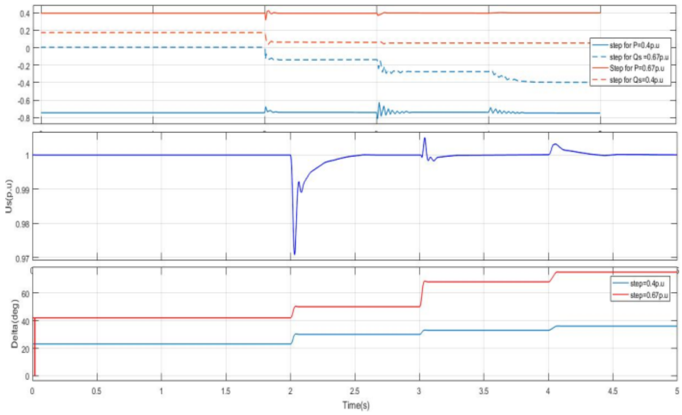

Fig.18 Disturbance resisting performance in the rectifier mode. Upper: active and reactive power injected by the VSC; middle: PCC voltage; lower: phase angle difference δ

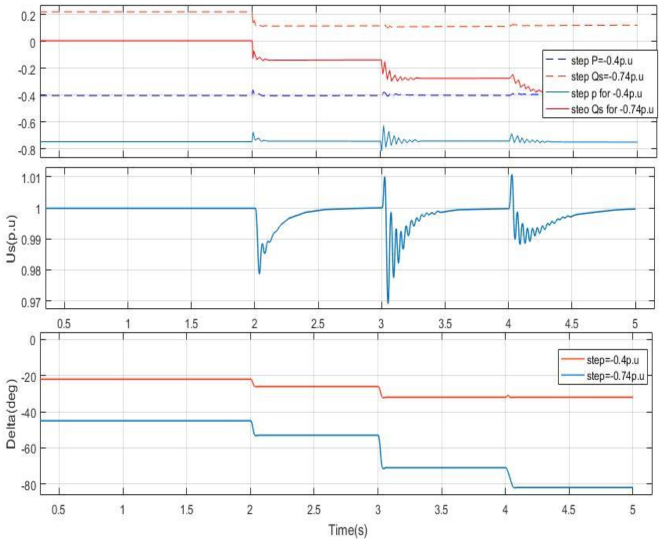

Fig.19 Disturbance resisting performance in the inverter mode. Upper: active and reactive power injected by the VSC; middle: PCC voltage; lower: phase angle difference δ.

CASE2: FUZZY Controller

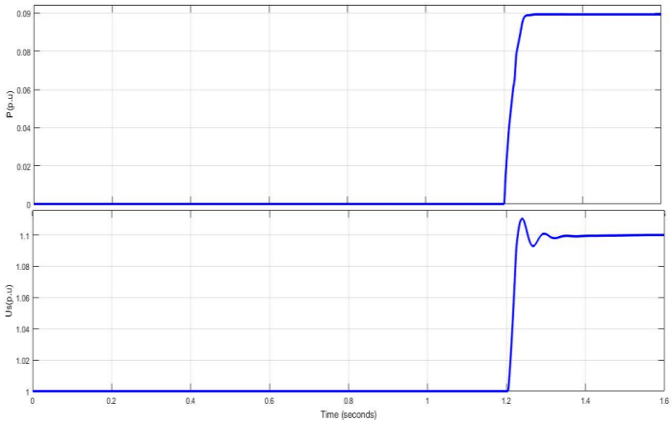

Fig.21 Dynamic Performance of the proposed method. Upper: Active Power Lower: PCC Voltage when Step 0.1p.u

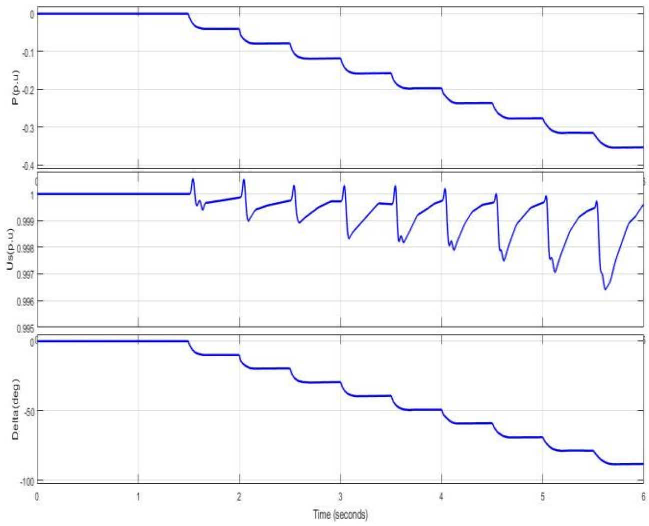

Fig.22 Stability Performance of the proposed method upper: active power at PCC; middle: PCC voltage; lower: phase angle δ. when K_{pac} = 0.005 , K_{iac} = 0.05

International Journal of Engineering Research & Technology (IJERT)
ISSN: 2278-0181
Vol. 8 Issue 11, November-2019

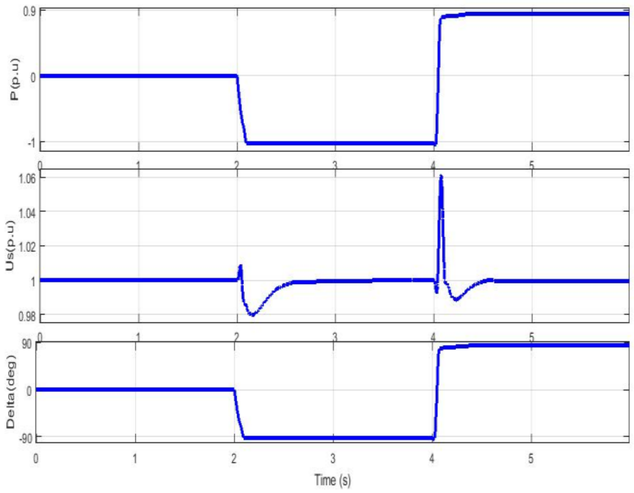

Fig.23 Limits testing of the proposed method. Upper: active and reactive power injected by VSC; middle: PCC voltage; lower: phase angle δ

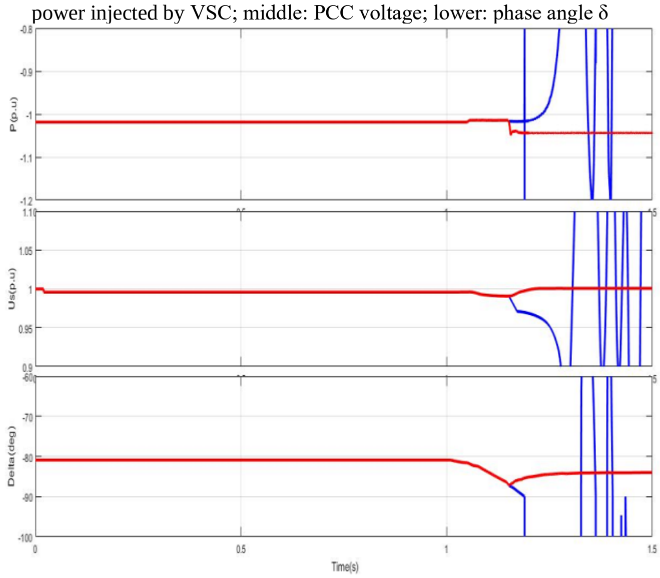

Fig.24 Damping performance of the proposed method for the step value of P= 1.04p.u upper: active power at PCC; middle: PCC voltage; lower: phase angle δ

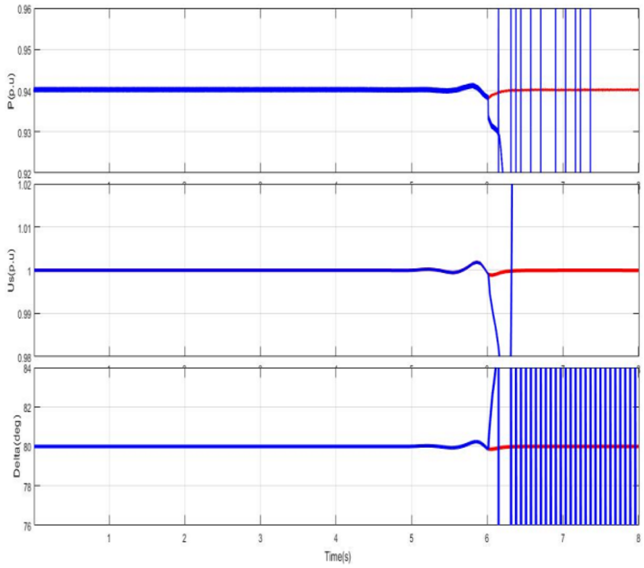

Fig.25 Damping performance of the proposed method for the step value of P= 0.94p.u upper: active power at PCC; middle: PCC voltage; lower: phase angle δ

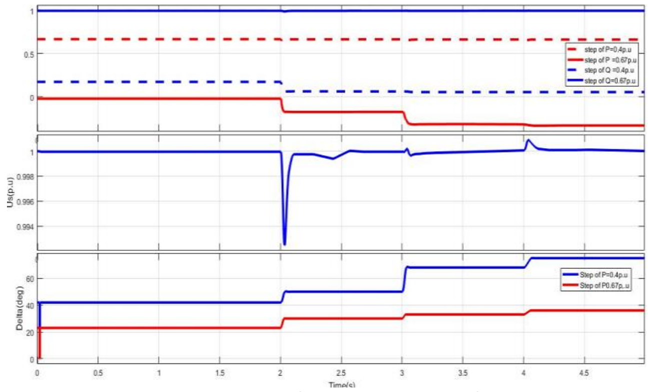

Fig.26 Disturbance resisting performance in the rectifier mode. Upper: active and reactive power injected by the VSC; middle: PCC voltage; lower: phase angle difference δ

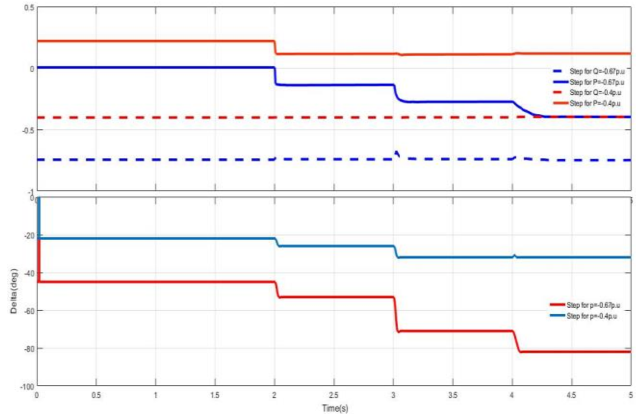

Fig.27 Disturbance resisting performance in the inverter mode of the proposed method. Upper: active and reactive power injected by the VSC; lower: phase angle difference δ

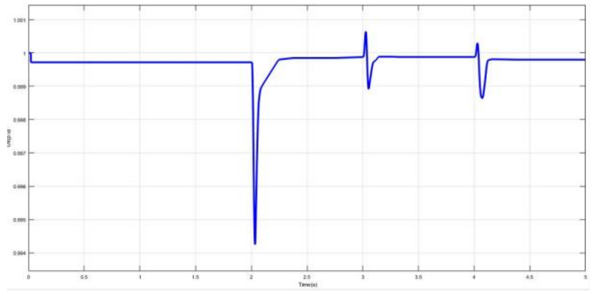

Fig.28 Disturbance resisting performance in the inverter mode of the proposed method.PCC Voltage

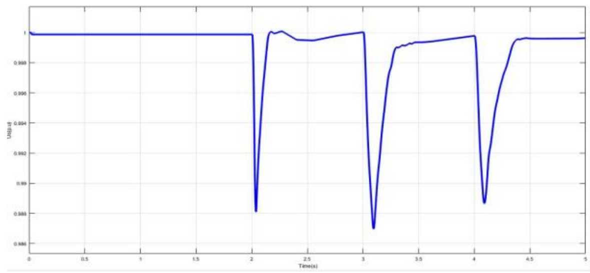

Fig.29 Disturbance resisting performance in the inverter mode of the proposed method.PCC Voltage

International Journal of Engineering Research & Technology (IJERT)
ISSN: 2278-0181
Vol. 8 Issue 11, November-2019

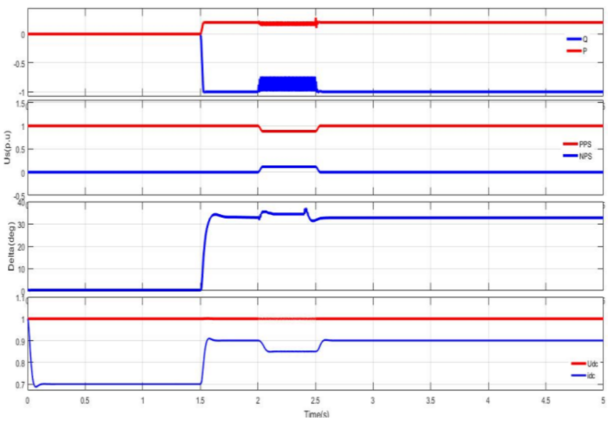

Fig.30 Fault ride-through performance of the proposed method. First: active and reactive power, second: voltages of P.S and NPS; third: phase angle δ; fourth: DC voltage and current.

5.3 Comparative Analysis

This section presents a comparative analysis between the traditional method and proposed method with respect to the time. From the above simulation results, we conclude that FUZZY controller is effectively controls and mitigate the Active power and PCC voltage when compared to PI controller. The Performance comparison of different control methods is shown

Table5.1 Dynamic performance comparison

Controller	Active Power(p.u)	PCC voltage(p.u)
PI	1	1.25
Fuzzy	0.98	1.15

Table 5.2 Comparison of the testing of the system

Controller	Active Power(p.u)	PCC voltage(p.u)
PI	1	1.18
Fuzzy	0.98	1.06

Table 5. 3 Comparison of disturbance rejection of a system

Controller	Rectifier Mode		Inverter Mode	
	Active Power	PCC voltage	Active power	PCC voltage
PI	0.6	0.97	0.6	0.96
Fuzzy	0.65	0.994	0.65	0.985

Table 5. 4 Comparison of fault analysis

Controller	Active Power(p.u)	PCC voltage(p.u)
PI	0.5	0.5
Fuzzy	0.2	0.2

VII. CONCLUSIONS

To enhance the operating limits and stability of VSCs which interconnect with weak power system, a power compensation control strategy combined with active damping control in inner loop has been proposed based on the analysis of PV curves. With the use of Fuzzy controller compensation strategy, the impact of compensation coefficients and steady state operating points on system performance has been studied based on the small signal model of the integrated system. The feasibility and effectiveness of the proposed control method has been validated. Electromagnetic transient simulation models are considered and verified in MATLAB/Simulink environment for the effectiveness of the method on the performance of operating limits, damping performance, disturbance withstanding capability, and fault ride-through capability.

REFERENCES

[1] D.P.Kothari, I.J.Nagrath "Modern Power System Analysis" Third Edition, New Age International Publisher, New Delhi.McGraw-Hill.2003

[2] C.L.Wadwa "Electrical Power Systems"11A Little Mount Sion, tun bridge walls,kent TN11YS US;2012

[3] Yunfeng Li, Guangfu Tang, Member, IEEE, Ting An, Hui Pang, Puyu Wang, Member, IEEE, Jie Yang, Yanan Wu, and Zhiyuan He, Member, IEEE " Power Compensation Control for Interconnection of Weak Power Systems by VSC –HVDC

[4] J. Sun, "Impedance based stability criterion for grid connected inverters,"IEEE Trans. Power Electron.,vol.26, no.11, pp.3075-3078, November 2011.

[5] T. An, X. Zhou, C. Han, Y. Wu, Z. He, H. Pang, and G. Tang, "A DC grid benchmark model for studies of interconnection of power system,"CSEE Jour. Energy Syst., vol.1, no.4, pp.101-109, Dec.2015.

[6] M. Guan, W. Pan, J. Zhang, Q. Hao, J. Cheng, and X. Zheng, "Synchronous generator emulation control strategy for voltage source converter (VSC) stations," IEEE Trans. Power Syst., vol. 30, no. 6, pp. 3093-3101, Nov. 2015

[7] J. He, and Y. Li, "Generalized closed loop control schemes with embedded virtual impedances for voltage source converters with LC or LCL filters," IEEE Trans. Power Electron., vol.27, no.4, pp.1850-1860,Apr. 2012.

[8] L. Zhang, L. Harnefors, and H. P. Nee, "Power synchronization control of grid connected voltage source converters ," IEEE Trans. Power Syst., vol. 25,no. 2, pp. 809-820, May 2010.

[9] M. Ashabani, and Y. Mohamed, "Integrating VSCs to weak grids by nonlinear power damping controller with self-synchronization capability," IEEE Trans. Power Syst., vol. 29, no. 2, pp. 805-814, Mar. 2014

[10] P. Mitra, L. Zhang, and L. Harnefors, "Offshore wind integration to a weak grid by VSC-HVDC links using power synchronization control: a case study, "*IEEE Trans. Power Del.*, vol. 29, no. 1, pp. 453-461, Feb. 2014.

[11] Q. Zhong, P. L. Nguyen, Z. Ma, and W. Sheng,"Self-synchronized synchronverters inverters without a dedicated synchronization unit," *IEEE Trans. Power Electron.*, vol. 29, no. 2, pp. 617-630, Feb. 2014.

[12] Egea-Alvarez, S. Fekriasl, F. Hassan, and O. Gomis-Bellmunt, "Advanced vector control for voltage source converters connected to weak grids," *IEEETrans. Power Syst.*, vol. 30, no. 6, pp. 3072-3081, Nov. 2015.

[13] Y. Huang, X. Yuan, J. Hu, and P. Zhou, "Modeling of VSC connected to weak grid for stability analysis of DC-Link voltage control," *IEEE J. Emerg.Sel. Topics Power Electron.*, vol. 3, no. 4, pp. 1193-1204, Dec. 2015.

[14] J. Zhou, H. Ding, S. Fan, Y. Zhang, and A. M. Gole, "Impact of Short-Circuit ratio and phase locked loop parameters on the small signal behavior of a VSC-HVDC converter," *IEEE Trans. Power Del.*, vol. 29, no. 5, pp.2287-2296, Oct. 2014.

[15] M. Ashabani, and Y. Mohamed, "Integrating VSCs to weak grids by nonlinear power damping controller with self-synchronization capability," *IEEE Trans. Power Syst.*, vol. 29, no. 2, pp. 805-814, Mar. 2014.

[16] P. Mitra, L. Zhang, and L. Harnefors, "Offshore wind integration to a weak grid by VSC-HVDC links using power synchronization control: a case study, "*IEEE Trans. Power Del.*, vol. 29, no. 1, pp. 453-461, Feb. 2014.

[17] Q. Zhong, P. L. Nguyen, Z. Ma, and W. Sheng,"Self-synchronized synchronverters inverters without a dedicated synchronization unit," *IEEE Trans. Power Electron.*, vol. 29, no. 2, pp. 617-630, Feb. 2014.

[18] M. Ashabani, and Y. Mohamed, "Novel comprehensive control framework for incorporating VSCs to smart power grids using

bidirectional synchronous-VSC," *IEEE Trans. Power Syst.*, vol. 29, no. 2, pp. 943-957, Mar. 2014.
[19] M. Ashabani, Y. Mohamed, M. Mirsalim, and M. Aghashabani "Multivariable droop control of synchronous current converters in weak grids," *IEEE Trans. Smart Grid*, vol. 6, no. 4, pp.1610-1620, Jul. 2015.
[20] J. Xu, S. Xie, T. Tang, "Active damping based control for grid connected LCL filtered inverter with injected grid current feedback only," *IEEE Trans. Ind. Electron.*, vol. 61, no. 9, pp. 4746-4758, Sep. 2014.
[21] X. Wang, Y. Li, F. Blaabjerg, and P. C. Loh, "Virtual Impedance-Based control for voltage source and current source converters," *IEEE Trans. Power Electron.*, vol. 30, no. 12, pp. 7019-7037, Dec. 2015.
[22] X. Wang, F. Blaabjerg, and P. C. Loh, "Grid current feedback active damping for LCL resonance in grid connected voltage source converters," *IEEE Trans.Power Electron.*, vol. 31, no. 1, pp. 213-223, Jan. 2016.
[23] D. Yang, X. Ruan, and H. Wu, "Impedance shaping of the grid connected inverter with LCL filter to improve its adaptability to the weak grid condition," *IEEE Trans. Power Electron.* vol. 29, no. 11, pp. 5795-5805, Nov. 2014.
[24] L. Xu, and L. Fan, "Impedance based resonance analysis in a VSC- HVDC system ," *IEEE Trans. Power Del.*, vol. 28, no. 4, pp. 2209-2216, Oct. 2013.
[25] L. Harnefors, A. G. Yepes, A. Vidal, and J. Doval-Gandoy, "Passivity based controller design of grid connected VSCs for prevention of electrical resonance instability ," *IEEE Trans. Ind. Electron.*, vol. 62, no. 2, pp. 702-710, Feb. 2015.
[26] J. He, Y. Li, D. Bosnjak, and B. Harris, "Investigation and active damping of multiple resonances in a parallel inverter based microgrid," *IEE Trans.Power Electron.*, vol. 28, no. 1, pp. 234-245, Jan. 2013.
[27] D. Pan, X. Ruan, C. Bao, W. Li, and X. Wang, "Capacitor current feedback active damping with reduced computation delay for improving robustness of LCL type grid connected inverter ", *IEEE Trans. Power Electron.*, vol. 29, no. 7, pp. 3414-3427, Jul. 2014.
[28] X. Guo, W. Wu, and Z. Chen, "Multiple complex coefficient filter based phase locked loop and synchronization technique for three phase grid interfaced converters in distributed utility networks ," *IEEE Trans. Ind. Electron.*, vol. 58, no. 4, pp. 1194-1204, Apr.2011.
[29] Suranjana Bharadwaj ," Application of Fuzzy Logic in Load Frequency Control of Two Area Power System" International Journal of Scientific & Engineering Research, Volume 5, Issue 11, November-2014

APPENDIX A
UTILISED PARK TRANSFORMATION

The used park transformation is defined as

$$|x_{dqo}| = |T(\theta)||x_{abc}| \qquad (24)$$

and the inverse is described as

$$|x_{abc}| = T(\theta)^{-1}|x_{dqo}| \qquad (25)$$

where$|x_{abc}|$ is a vector with the three-phase quantities in the dq0frame and is a vector with the transformed quantities in the frame.

The transformation $[T_{dq0}]$ matrix can be written as

$$[T(\theta)] = \frac{2}{3}\begin{bmatrix} \cos\theta & \cos(\theta - \frac{2\pi}{3}) & \cos(\theta + \frac{2\pi}{3}) \\ \sin\theta & \sin(\theta - \frac{2\pi}{3}) & \sin(\theta + \frac{2\pi}{3}) \\ \frac{1}{2} & \frac{1}{2} & \frac{1}{2} \end{bmatrix} \qquad (26)$$

and its inverse

$$[T(\theta)]^{-1} = \frac{2}{3}\begin{bmatrix} \cos\theta & \sin\theta & 1 \\ \cos(\theta - \frac{2\pi}{3}) & \sin(\theta - \frac{2\pi}{3}) & 1 \\ \cos(\theta + \frac{2\pi}{3}) & \sin(\theta + \frac{2\pi}{3}) & 1 \end{bmatrix} (27)$$

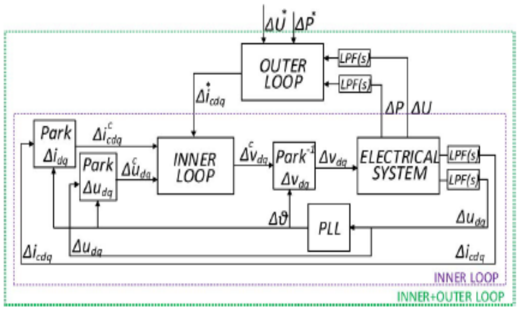

Fig. 31. Scheme of the linearized system

APPENDIX B
LINEARIZED DYNAMIC EQUATIONS

The dynamic system equations are linearized as independent systems and they are connected according to Fig. 31 for the inner loop and outer loop control. The subscript indicates the value at the linearization point, indicates an average of the variable quantity and the superscript means that the variables have been transformed by means of the linearized park transformation

1) Linearized Electrical System Equations: The electrical system is composed by the coupling filter and the electrical gridn(see Fig. 1). The state space representation of the linearized system is defined by

$$\Delta_{\dot{x}} = A_{lc}\Delta x_{lc} + B_{lc}\Delta u_{lc} \qquad (28)$$

$$\Delta Y = c_{lc}\Delta x_{lc} \qquad (29)$$

Where the state variables , inputs and outputs are

$$\Delta_{ulc} = \left[\Delta v_d \; \Delta v_q \; \Delta e_d \; \Delta e_q\right] \qquad (30)$$

$$\Delta_{ylc} = \left[\Delta i_{cd} \; \Delta i_{cq} \; \Delta u_d \; \Delta u_q \; \Delta u \; \Delta P\right] \qquad (31)$$

Where the matrix C_{lc} is defined as

$$C_{lc} = \begin{bmatrix} 1 & 0 & 0 & 0 & 0 & 0 \\ 0 & 1 & 0 & 0 & 0 & 0 \\ 0 & 0 & 1 & 0 & 0 & 0 \\ 0 & 0 & 0 & 1 & 0 & 0 \\ 0 & 0 & \frac{u_{do}}{U_0} & \frac{u_{q0}}{U_0} & 0 & 0 \\ 0 & 0 & \frac{3i_{ndo}}{2} & \frac{3i_{nq0}}{2} & \frac{3u_{do}}{2} & \frac{3u_{q0}}{2} \end{bmatrix} \qquad (32)$$

2) Linearized PLL Equations: The PLL is used in order to orient a control with the electrical grid angle. In the linearized model the PLL introduces the angle deviation when the linearized system is moved from the linearization point. The PLL has been linearized following [11]. The PLL linearised transfer function representation is

$$\Delta\theta = -\frac{k_p{-}plls + k_i{-}pll}{s^2 + u_{do}k_p{-}plls + u_{do}k_i{-}pll}\Delta u_q \qquad (33)$$

3). Linearized Park Transformation and Inverse-Transformation Equations: The linearized Park transformation (see Appendix B) expressed is given by

$$\left[x^c{}_{dq}\right] = \left[T^c{}_{dq}\right]\left[\Delta x_d \; \Delta x_q \; \Delta\theta\right]^T \qquad (34)$$

Where $\left[T^c_{dq}\right]$ is

$$\left[T^c_{dq}\right] = \begin{bmatrix} \cos\theta_0 & -\sin\theta_0 & -\sin\theta_0\, x_{d0} - \cos\theta_0\, x_{q0} \\ \sin\theta_0 & \cos\theta_0 & \cos\theta_0\, x_{d0} - \sin\theta_0\, x_{q0} \end{bmatrix} (35)$$

and the linearized inverse transformation is

$$\left[x_{dq}\right] = \left[T^c{}_{dq}\right]^{-1}\left[\Delta x^c{}_d \; \Delta x^c{}_q \; \Delta\theta\right]^T \qquad (36)$$

Where $T\left[T^c_{dq}\right]^{-1}$ is

$$[T^c_{dq}]^{-1} = \begin{bmatrix} \cos\theta_0 & \sin\theta_0 & \cos\theta_0\, x_{d0} - \sin\theta_0\, x_{q0} \\ -\sin\theta_0 & \cos\theta_0 & -\cos\theta_0\, x_{d0} - \sin\theta_0\, x_{q0} \end{bmatrix} \quad (37)$$

4) Inner Loop Equations: The vector current control equations are

$$\Delta\dot{x}_{il} = B_{il}\Delta u_{il} \quad (38)$$

$$\Delta y_{il} = C_{il}\Delta x_{il} + D_{il}\Delta u_{il} \quad (39)$$

Where the state variables, inputs and outputs are

$$\Delta x_{il} = [\Delta e{i^c}_{cd}\ \Delta e{i^c}_{cq}] \quad (40)$$

$$\Delta u_{il} = [\Delta {i^*}_{cd}\ \Delta {i^*}_{cq}\ \Delta {i^c}_{cd}\ \ \Delta {i^c}_{cd}\ \ \Delta {i^c}_{cq}\ \ \Delta {u^c}_{d}\ \ \Delta {u^c}_{q}] \quad (41)$$

$$\Delta y_{il} = [\Delta {v^c}_{d}\ \Delta {v^c}_{q}] \quad (42)$$

Δei_{cdq} is the current error, defined as the difference between $\Delta {i^*}_{cdq}$ and $\Delta {i^c}_{cdq}$. The matrix gains are

$$B_{il} = \begin{bmatrix} -1 & 0 & 1 & 0 & 0 & 0 \\ 0 & -1 & 0 & 1 & 0 & 0 \end{bmatrix} \quad (43)$$

$$C_{il} = \begin{bmatrix} k_i & 0 \\ 0 & k_i \end{bmatrix} \quad (44)$$

$$D_{il} = \begin{bmatrix} -k_p & 0 & k_p & -\omega L_c & 1 & 0 \\ 0 & -k_p & \omega L_c & k_p & 0 & 1 \end{bmatrix} \quad (45)$$

5) Classic Outer Loop Equations: For the study of the whole classic system, the outer loop equations are

$$\Delta\dot{x}_{ol} = B_{ol}\Delta u_{ol} \quad (46)$$

$$\Delta y_{ol} = C_{ol}\Delta x_{ol} + D_{ol}\Delta u_{ol} \quad (47)$$

where the state variables, inputs, and outputs are

$$\Delta x_{ol} = [\Delta e_p\ \ \Delta e_u] \quad (48)$$

$$\Delta u_{ol} = [\Delta P^*\ \ \Delta U^*\ \ \Delta P\ \ \Delta U] \quad (49)$$

$$\Delta y_{ol} = [\Delta {i^*}_{cd}\ \ \Delta {i^*}_{cq}] \quad (50)$$

ΔeP and ΔeU are the active power and ΔU voltage error.

Where the matrix gains are defined as

$$B_{ol} = \begin{bmatrix} 1 & 0 & -1 & 0 \\ 0 & 1 & 0 & -1 \end{bmatrix} \quad (51)$$

$$C_{ol} = \begin{bmatrix} k_{i-p} & 0 \\ 0 & k_{i-u} \end{bmatrix} \quad (52)$$

$$D_{ol} = \begin{bmatrix} k_{p-p} & 0 & -k_{p-p} & 0 \\ 0 & k_{i-u} & 0 & -k_{i-u} \end{bmatrix} \quad (53)$$